Prediction of small quadrotor blade induced noise

Austin D. Thai* and Sheryl M. Grace†
Boston University, Boston, Massachusetts, 02215

Noise predictions for a small quadrotor rotor in hover are performed using high-fidelity computational fluid dynamics (CFD) analysis together with a Ffowcs Williams-Hawkings (FWH) solver. The aerodynamic performance for the DJI Phantom 3, both in quadrotor and isolated rotor configurations, is computed using CREATE^{TM}-AV Helios. The surface pressure distribution for the isolated rotor acts as input to the acoustic calculation, which is an implementation of the steady, farfield, terms in Farassat Formulation 1A. The predicted sound field agrees well with expected directivity patterns for thickness and loading acoustic pressure. The results are compared with experimental data and the computational methodology is shown to be robust.

Nomenclature

A	=	rotor planform area, m^2
c	=	chord, m
η	=	figure of merit
f	=	surface defining function
M	=	Mach number
Ω	=	rotation rate, rad/s
p	=	pressure, Pa
p'_L	=	acoustic loading pressure, Pa
p'_T	=	acoustic thickness pressure, Pa
ρ_0	=	fluid density, kg/m^3
ρ	=	air density, kg/m^3
r	=	distance between source and observer, m
R	=	rotor radius, m
τ	=	torque about the axis of rotation, $N \cdot m$
θ	=	angle between surface normal and radiation direction, rad
t	=	time, s
T	=	thrust, N
SPL	=	sound pressure level, dB
y^+	=	dimensionless wall spacing

I. Introduction

Applications for small quadrotors such as surveillance, remote photography, recreation, and even package delivery motivate the study of their performance and noise characteristics. The noise attributed to the rotors has both tonal and broadband components and is unfortunately aligned perfectly with human perception so as to make the noise particularly annoying [1, 2]. The main sources of quadrotor noise are the electric motors and the rotors. Prediction of the quadrotor performance and production of tonal noise due to the rotors is the focus of this work.

Several recent papers focus on experimentally quantifying the aerodynamic performance of commercially available quadrotors [3–5]. In addition, a few studies have investigated the noise associated with a small quadrotor [3, 6–8]. However, experiments are limited by testing conditions and it is often difficult to identify design flaws due to a lack of detailed flow visualization and the difficulties in obtaining surface pressure distributions. Therefore, in some sense, experiments only aid in the evaluation of design rather than provide direct design feedback, and it is beneficial to have

*Graduate Student, Mechanical Engineering Department, 110 Cummington Mall, AIAA Student Member.
†Associate Professor, Mechanical Engineering Department, 110 Cummington Mall, AIAA Associate Fellow.

reliable computational tools that can assess both the aerodynamic effects and the noise that will be produced by a particular design.

Recently, the National Aeronautics and Space Administration (NASA) has taken an interest in small vertical lift vehicles, and funded several projects concerning multirotor aerodynamics and aeroacoustics [4, 5, 9–12]. Influences on aerodynamic performance and noise were studied including the influence of quadrotor orientation in flight on performance and rotor separation distance on noise. A summary of the efforts in acoustics is given by Zawodny et al. [13] and a summary of the Design Environment for Novel Vertical Lift Vehicles (DELIVER) project as a whole is given by Theodore [14].

The majority of the computational work performed by NASA used the CFD codes FUN3D and OVERFLOW. This work expands the quadrotor noise prediction capability to mStrand, a strand-grid flow solver. In particular, mStrand [15] will be coupled to CREATE^{TM}-AV Helios, a rotorcraft simulation suite that is developed by the U.S. Army Aviation Development Directorate [16, 17].

In this research, the two step approach to noise modeling is applied. A high fidelity CFD analysis is first performed to obtain the surface pressure distribution on the quadrotor and then the FWH equation is used to determine the acoustic field based on a steady surface pressure. The acoustic analysis is performed using an in-house implementation of Farassat's Formulation 1A of the FWH equation [18–21].

The DJI Phantom 3 serves as the quadrotor platform for this study. Background on computational rotorcraft predictions is given in Section II. The computational methods are described in Section III. Section III.C describes the experimental performance and noise data that are available for validation. The verification and validation of the computational method is then discussed in Section IV.

II. Background

Researchers have been successful in the past with predicting helicopter noise using PSU-WOPWOP, a FWH solver [22–24], coupled to a near field solver. In fact, Helios has already been used with PSU-WOPWOP to predict blade vortex interaction noise for a coaxial helicopter [25]. The previous work focused on helicopters and as such involved high Mach number and high Reynolds number flows. Small quadrotor aerodynamics, of interest in this work, is characterized by low Mach number and low Reynolds number. Helios-mStrand has not been validated in this regime previously, nor has it been coupled to a FWH computation for the acoustics. This paper begins the validation process by considering the prediction of performance parameters and noise associated with a small quadrotor in hover.

The DJI Phantom 3 was chosen as a characteristic quadrotor geometry due to its commercial popularity and detailed performance database. Scientists at NASA Ames Research Center tested both the quadrotor and isolated rotor configurations of this quadrotor [4, 5], and provided the laser scanned computer-aided design model used to generate the meshes for this study. The plastic 9450 rotors used in the study have an average chord of approximately 2.5 cm and a rotor radius of 12 cm. The fuselage has a length (along the arm) of 0.39 m. The range of tested RPMs were between 2500 and 8000, resulting in tip Mach numbers between 0.09 and 0.3. In this study, the rotor disk was chosen to lie in the X-Y plane, with the Z-axis as the axis of revolution. To be able to validate the computations with experiments, four RPMs within the test range were simulated: 3000, 3500, 5000, and 7000.

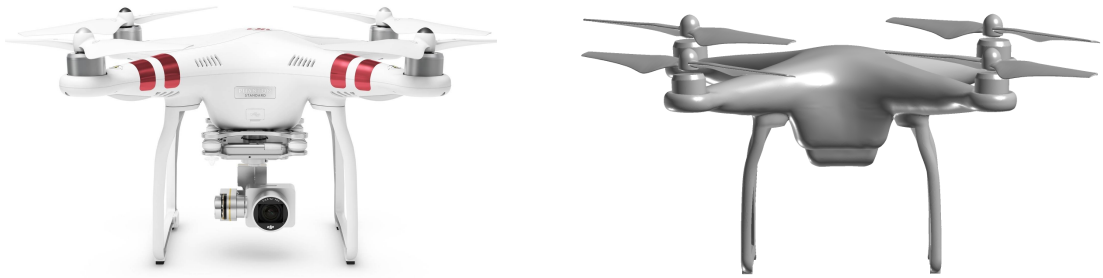

(a) Vendor model [26] **(b) CAD model**

Fig. 1 DJI Phantom 3 geometry.

III. Computational methods

A. CREATE^{TM}-AV Helios

The CREATE^{TM}-AV Helios suite of codes is developed and maintained by the U.S. Army's Aviation Development Directorate, part of the Combat Capabilities Development Command Aviation and Missile Center. Helios is a high-fidelity overset CFD code and uses SAMCART, a structured high-order Cartesian flow solver, for the off-body volume mesh. SAMCART is capable of geometry adaptation and adaptive mesh refinement. Although Helios is capable of using NASA FUN3D or NASA OVERFLOW as its near body solver, Helios has a native flow solver, mStrand, that is capable of automatic volume mesh generation. mStrand was chosen for this study because it has yet to be used in small quadrotor noise predictions. Several other modules that Helios implements are: PUNDIT, which provides domain connectivity for parallel computing, overset interpolation, and implicit hole cutting; COVIZ, which enables runtime data extraction for postprocessing; and MELODI, which defines bodies and their relative motions, including spanwise air loads for rotors. MELODI is also capable of aeroelastic motion and CFD/CSD coupling for deformations, but these features are not relevant for current simulations.

In this research, the grids are generated using Pointwise and the visualization is performed with Fieldview by Intelligent Light. The Reynolds-Averaged Navier-Stokes (RANS) equations are implemented in mStrand, but they require closure of the Reynolds stress term. In a previous study on quadrotor CFD, the Spalart Allmaras Detached Eddy Simulation (SA-DES) turbulence model demonstrated the best results based on the accuracy of thrust predictions and computational efficiency [27]. Therefore, the SA-DES model was chosen for this study. The near body volume mesh is trimmed up to 0.4c and the off-body volume mesh is extended to 10 times the rotor radius. There are four overset layers between the near-body and off-body meshes.

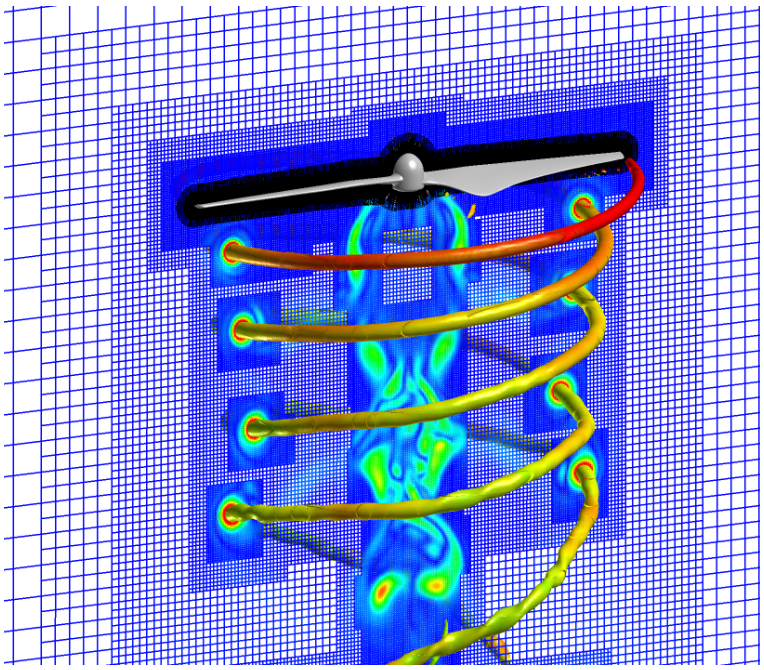

Fig. 2 Isolated rotor simulation visualization of the iso-surfaces of Q-criterion juxtaposed on the coordinate surface of the Y-Z plane, colored by vorticity magnitude. The black coordinate surface on the rotor is a slice of the mStrand volume mesh.

The first ten rotor revolutions, simulated with a 2.5 degree azimuth time step, are followed by three rotor revolutions with a 0.25 degree azimuth time step. The coarser initial time stepping allows for transient computational effects to quickly dissipate and speeds up convergence towards a steady hover prediction. Adaptive mesh refinement is generally not initialized at the beginning of the simulation due to the uncertainties of the starting vortex, and therefore was turned on after the first ten rotor revolutions to save computational resources. This time-stepping methodology was previously validated for rotorcraft and is shown to be robust [27]. The converged thrust and moment used for the figure of merit

were calculated as the average value over the final rotor revolution.

The mesh for the rotor and the fuselage is identical to that used by Thai et al. [27]. The surface spacing is 0.03c for the rotor and 0.05c for the fuselage. The trailing edge spacing for the rotor is 0.0002c and the leading edge spacing is 0.0001c. The near-body volume meshes, which were automatically generated by mStrand, have 31 normal points, a total extrusion distance of 0.4c, and a normal spacing that satisfies $y^+ < 1$. Flow visualization for the last time step in the isolated rotor simulation can be seen in Fig. 2. The vortical structures are the iso-surfaces of Q-criterion colored by vorticity magnitude, with red indicating high vorticity. The black mesh corresponds to mStrand while the blue mesh corresponds to SAMCART. There is evidence of adaptive mesh refinement in the regions of high vorticity.

The CFD calculations discussed in this paper were all performed in parallel on the Department of Defense High Performance Computing cluster Conrad, with Intel Xeon E5-2698v3 processors. 800 processors were used for the isolated rotor simulations while 960 processors were used for the quadrotor simulation.

B. Aeroacoustics Solver

The noise generated by an isolated rotor in a quiescent field can be computed based on the rotor's surface pressure distribution and the rotor's rotation rate. In this study, the FWH equation is solved using Farassat Formulation 1A (FF1A) [19–21]. The thickness and loading acoustic pressure components are listed below as shown in [21]:

$$4\pi p'_T(x,t) = \int_{f=0} \left[\frac{\rho_0 \dot{v}_n}{r(1-M_r)^2} + \frac{\rho_0 v_n \hat{r}_i \dot{M}_i}{r(1-M_r)^3} \right]_{\text{ret}} dS + \int_{f=0} \left[\frac{\rho_0 c v_n (M_r - M^2)}{r^2(1-M_r)^3} \right]_{\text{ret}} dS, \tag{1}$$

$$4\pi p'_L(x,t) = \int_{f=0} \left[\frac{\dot{p}\cos\theta}{cr(1-M_r)^2} + \frac{\hat{r}_i \dot{M}_i p \cos\theta}{cr(1-M_r)^3} \right]_{\text{ret}} dS + \int_{f=0} \left[\frac{p(\cos\theta - M_i n_i)}{r^2(1-M_r)^2} + \frac{(M_r - M^2) p \cos\theta}{r^2(1-M_r)^3} \right]_{\text{ret}} dS. \tag{2}$$

In Eq. 1-2, p'_T is the acoustic thickness pressure, p'_L is the acoustic loading pressure, ρ_0 is the fluid density, v_n is body's normal velocity component, $\hat{r}_i$ is the radiation vector, r is the distance between the source and observer, p is the surface pressure, M_i is the vectorized Mach number, M_r is the radiation Mach number, and θ is the angle between the surface normal and the radiation vector. This formulation is the same as the one used in PSU-WOPWOP.

Ideally, a hovering rotor experiences a uniform steady loading due to symmetry in the rotor plane. In this study, the pressure in hover is assumed to be steady, and the surface pressure distribution is extracted from the final time step of the simulation, at the end of the last rotor revolution. Therefore, the time derivative terms in FF1A are identically zero, and only the steady, farfield terms remain. The resulting equations for thickness and loading acoustic pressure can be rewritten as:

$$4\pi p'_T(x,t) = \int_{f=0} \left[\frac{\rho_0 c v_n (M_r - M^2)}{r^2(1-M_r)^3} \right]_{\text{ret}} dS, \tag{3}$$

$$4\pi p'_L(x,t) = \int_{f=0} \left[\frac{p(\cos\theta - M_i n_i)}{r^2(1-M_r)^2} + \frac{(M_r - M^2) p \cos\theta}{r^2(1-M_r)^3} \right]_{\text{ret}} dS. \tag{4}$$

In this study, the rotor blade is impermeable, and the $f = 0$ surface for the integral is the rotor surface. The subscript "ret" signifies retarded time. Although a source time algorithm has been shown to be less computationally intensive, the blade motions in hover are fairly simple and therefore a retarded time algorithm was implemented.

The aeroacoustics calculations were performed in serial on high memory nodes on the Shared Computing Cluster at Boston University with Intel Xeon E5-2680v4 processors.

C. Experimental data

Performance data for the DJI Phantom 3 with 9450 rotors in hover and in forward flight were obtained by researchers at NASA Ames as part of the Design Environment for Novel Vertical Lift Vehicles (DELIVER) project, the UAS Traffic Management (UTM) project, and the Revolutionary Vertical Lift Technology (RVLT) project [4, 5]. The quadrotor was installed on the wind tunnel sting assembly at a 90-degree right roll angle so that flight conditions at different vehicle angles of attack could be achieved using the tunnel turntable. For this paper, only the hover (no wind) condition is of interest. The wind tunnel was not required to obtain hover data and as such hover data were acquired with the quad on the same sting assembly but placed in the middle of a large laboratory. Forces and moments were measured using a six-axis load cell manufactured by JR3 Inc. In addition to full quadrotor measurements, single rotor thrust measurements were also made.

Performance and noise data for the DJI Phantom 2 in hover with several different rotors including the 9450 (original) and the 9443 (aftermarket) were obtained in the VT Anechoic Chamber [3]. Thrust was recorded using a LC101-25 Omega S-beam load cell. The quadrotor was attached at a 0-degree roll angle such that the axis of the load cell was aligned with the center of the quadrotor. The bottom of the quadrotor was 0.77m away from the chamber grate floor. Acoustic measurements were made with a single 1/2" Bruel and Kjaer 4190 microphone. It was placed 0.767 m below the top of the quadrotor fuselage and 1.295 m to the side, resulting in approximately a 50 degree directivity angle approximately. This microphone location will be mimicked in this study. Although the geometry of this study and the one used in the current study are not identical, they belong to the same line of models produced by DJI and should serve as a good basis for comparison.

IV. Results

A. Aerodynamics Results

1. Isolated rotor

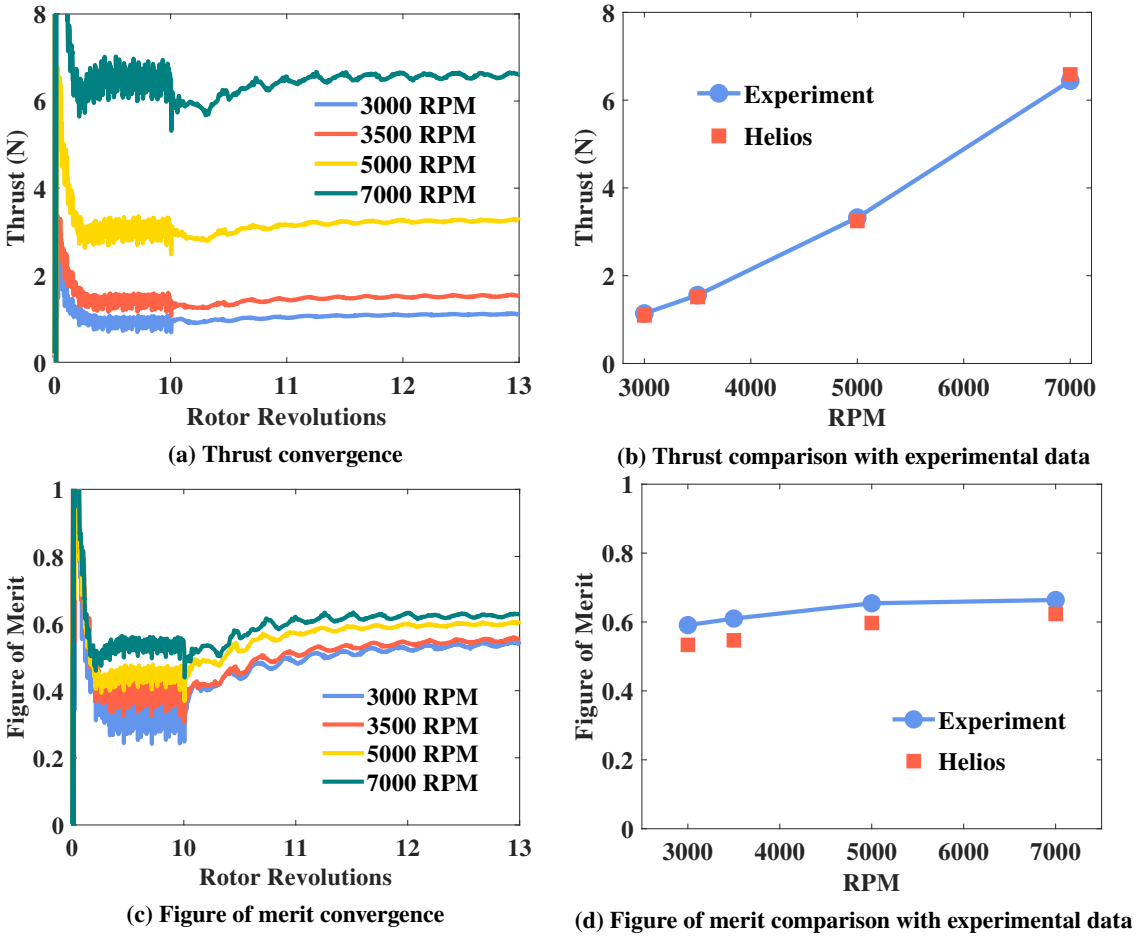

(a) Thrust convergence

(b) Thrust comparison with experimental data

(c) Figure of merit convergence

(d) Figure of merit comparison with experimental data

Fig. 3 Isolated rotor results.

The results of the Helios-mStrand simulations are reported in this section. An RPM sweep of the isolated rotor configuration was conducted to obtain a trendline for comparison with experimental data. The convergence of the thrust value over the simulation period can be seen in Fig. 3a. The predicted thrust is highly erratic over the first ten rotor revolutions due to the coarse time-stepping, but after the time-stepping is adjusted, the thrust value appears to converge and becomes steady over the final rotor revolution. The amplitude of the periodicity in the thrust signals increases with

RPM, likely due to the increase in turbulence. The converged thrust values are plotted against experimental data in Fig. 3.

The figure of merit, a measure of rotor efficiency, was calculated using:

$$\eta = \frac{T}{\Omega\tau}\sqrt{\frac{T}{2\rho A}}, \tag{5}$$

where T is the thrust, Ω is the rotor rotation rate, τ is the torque, ρ is the density of air, and A is the rotor planform area. While the thrust prediction is quite good, there is a noticeable underprediction of the figure of merit, plotted against experimental data in Fig. 3c. It was surmised that the torque is inaccurately predicted because of the need for a transition model when in this lower Reynolds' number regime. However, a recent study showed that the inclusion of a standard transition model did significantly change the results [27]. It should also be noted that all of the reported computational results are well within the experimental uncertainty reported by Russell et al. [5]. Therefore, it is difficult to conclude, to a high degree of accuracy, the validity of the models. This remains an open research question. Overall, the magnitude and trends of this study are reasonable and the surface pressures should be appropriate for use in an acoustic prediction.

The surface pressure distribution extracted from the CFD simulation is extremely important because it is directly used in the prediction of the sound field. The top and bottom views of the instantaneous pressure distribution on the rotor blade is plotted in Fig. 4. The figures shown are the final time step of the simulation and directly correspond to the values used in the aeroacoustics analysis section of this paper. The figures are all plotted on the same scale with red corresponding to high pressure and blue corresponding to low pressure. In general, an increase in RPM causes an increase in thrust, so the difference in pressure between the top and bottom surface increases.

Quadrotors are trimmed by changing the RPM of their rotors instead of varying the collective or cyclic pitch angles like helicopters. It is therefore desirable to create a uniform lift distribution on the rotor. Such a uniform disk of thrust is achieved by varying the chord length and twist according to spanwise distance. The result of these design choices are made apparent by the change in pressure along the rotor blade in Fig. 4. This effect is most noticeable in the 7000 RPM case when the color changes from yellow to blue from hub to tip on the top surface but yellow to red from hub to tip on the bottom surface while the rotor geometry is tapered and twisted from hub to tip.

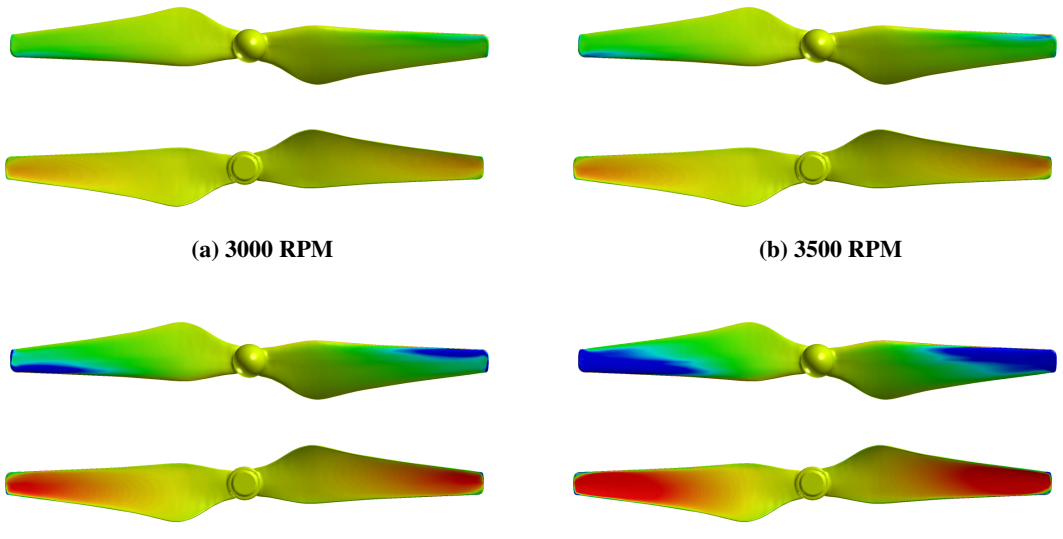

(a) 3000 RPM **(b) 3500 RPM**

(c) 5000 RPM **(d) 7000 RPM**

Fig. 4 Top and bottom views of the instantaneous pressure on the isolated rotor at the final time step, red corresponds to high pressure and blue corresponds to low pressure.

2. Quadrotor

Full quadrotor simulations were performed using the same set of RPMs as the isolated rotor simulations. Although the experimental data set did not extend below 3500 RPM, a simulation was conducted at 3000 RPM to provide a dataset for comparison with the isolated rotor results. The thrust is plotted against experimental data in Fig. 5a, and shows very good agreement across all RPMs. Therefore, it seems that the rotor-fuselage interactional effects were properly characterized by the simulation. Although the download was not measured experimentally, the percentage of the component of download in the total thrust was plotted as a function of RPM in Fig. 5b. The decrease in the significance of the download indicates the ability for the flow field to overcome blockage at higher Reynold's number. This is similar to flow reattachment with the onset of turbulence, resulting in decreased drag, for the fundamental study involving flow past a circular cylinder.

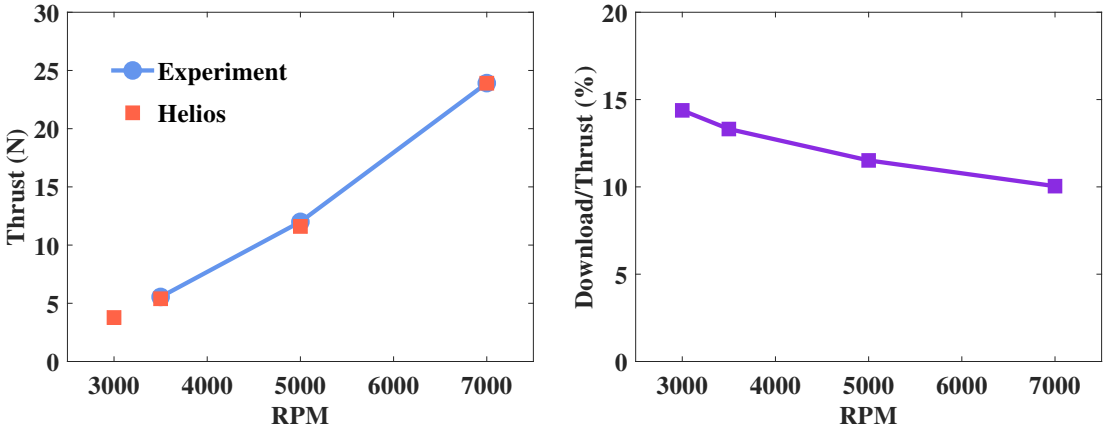

(a) Thrust comparison with experimental data **(b) Download as a percentage of thrust**

Fig. 5 Quadrotor results.

In Fig. 6, the iso-surface of Q-criterion is plotted for the 3500 and 7000 RPM cases from the quadrotor simulation. The figures are colored by vorticity magnitude, and the higher Reynolds number flow clearly increases the amount of vortical structures. In addition, there is an interesting amalgamation of vortices in the center of the top of the fuselage, where the rotor-tip passes. The rotors were set up in phase, and these interactions between multiple rotors and the airframe will have an impact on the aerodynamic performance. A previous study showed that rotor-fuselage height variation demonstrates nonlinear effects on thrust production due to a combination of flow reingestion, fuselage effect, and download [28].

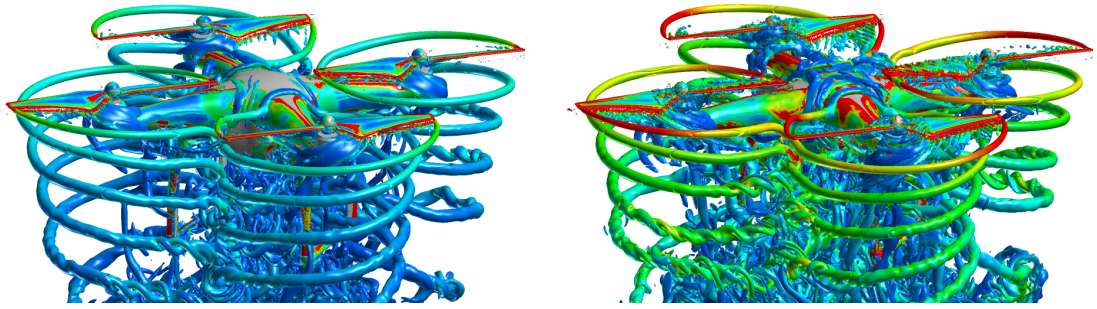

(a) 3500 RPM **(b) 7000 RPM**

Fig. 6 Iso-surface of Q-criterion, colored by vorticity magnitude, for the quadrotor simulations.

B. Aeroacoustics Results

The tonal noise produced by the isolated rotor in hover is considered in this paper. Microphones were simulated 16R away from the center of the rotor to agree with Zawodny et al. [10], with the exception of a seventh location, which was

chosen to agree with the measurement location in Ref. [3]. The observer locations can be found in Table 1. The acoustic pressure associated with the steady loading is plotted in Fig. 7 while the acoustic pressure due to the thickness effect is plotted in Fig. 8. The loading acoustic pressure is greater than the thickness acoustic pressure. Acoustic pressure, across all observers, increases with RPM, as expected.

Table 1 Observer locations.

Observer	x	y	z	*r*	Description
1	0	0	1.92	16R	Directly above the rotor
2	0	0	-1.92	16R	Directly below the rotor
3	0	1.7338	-0.7348	16R	22.5° below the rotor plane
4	0	1.3576	-1.3576	16R	45° below the rotor plane
5	0	1.92	0	16R	In the rotor plane
6	0.96	0.96	-1.3576	16R	45° azimuth from observer 4
7	0	1.295	-0.767	12.5R	Matches Intaratep et al. [3]

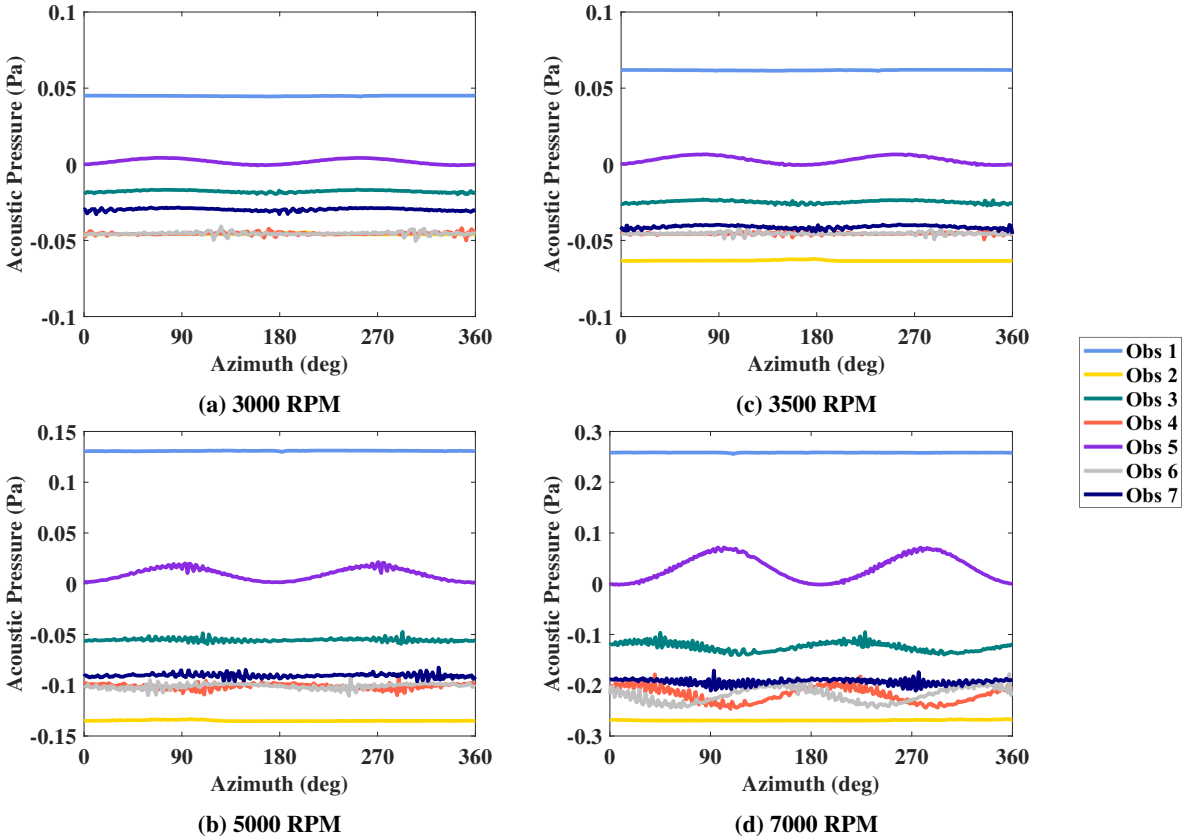

Fig. 7 Isolated rotor acoustic loading pressure.

In Fig. 9, the frequency spectrum of the SPL for each of the isolated rotor simulations is plotted for two locations: observer 5 and observer 7. Due to the steady nature of hovering flight and the assumptions made for the acoustics analysis, the sound pressure spectrum in time was assumed to be periodic. Therefore, before computing the Fast Fourier Transform (FFT), the signal was repeated twenty times so that the amplitude is retained. Overall, the frequency spectrum yields only tonal components, as the broadband noise cannot be predicted in a steady simulation. Observer 5 demonstrated the highest sound overall with a strong first BPF harmonic. At this microphone location, the first BPF

harmonic dominates the spectrum. The amplitude of the sound increases with RPM. There is noticeable noise at higher frequencies, most likely due to the unsteadiness from the acoustic thickness predictions.

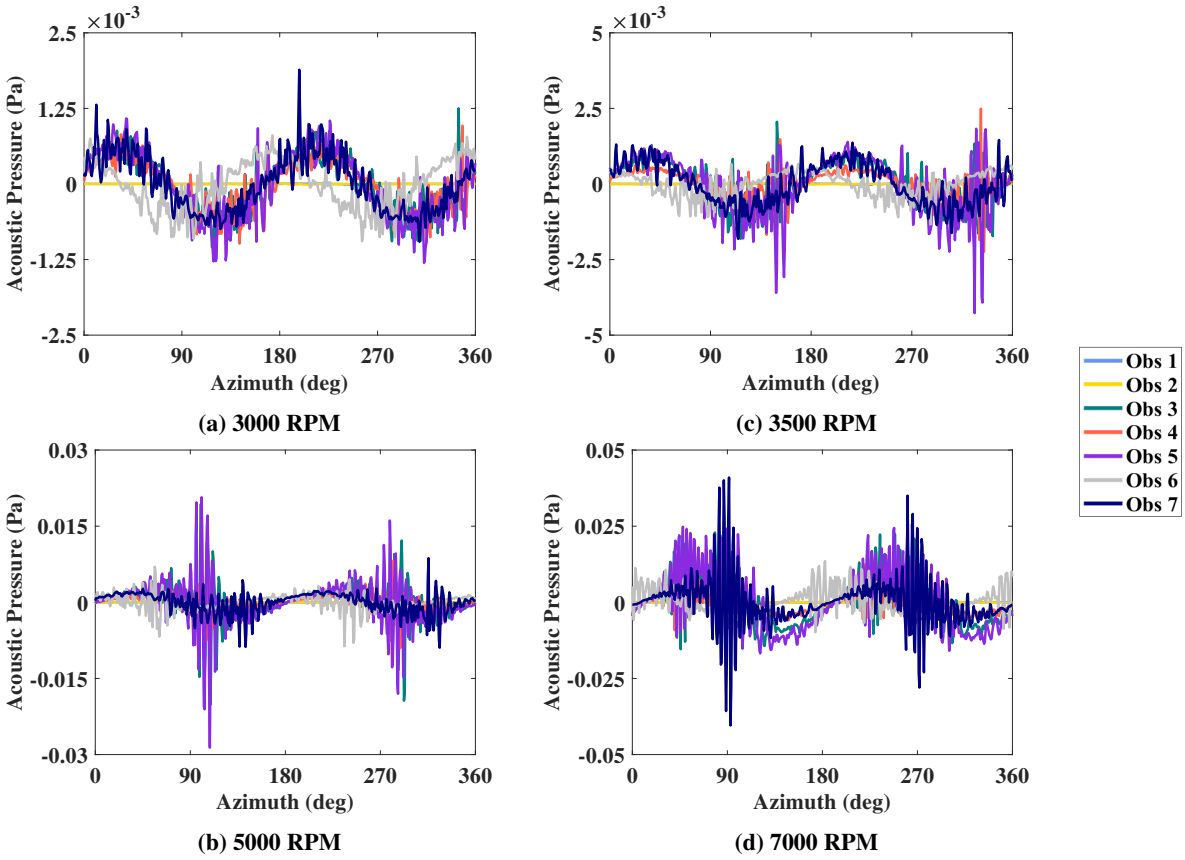

Fig. 8 Isolated rotor acoustic thickness pressure.

Observer 7, which is placed in the same location as the microphone by Intaratep et al. [3], shows similar tonal characteristics as the previous study. Several comparisons can be made between the frequency spectra in both studies. The observer experiences the greatest sound at the first BPF harmonic, as previously determined. Also, there is a general increase in the SPL as the rotor RPM increases. Intaratep et al. demonstrated approximately a 20 dB increase in SPL at the first BPF harmonic between 4000 and 6000 RPM, and this study shows a 13 dB increase. It is important to note that the single rotor experiments conducted in the previous study were not isolated rotor, but rather a mounted quadrotor with a single actuated rotor. The rotor-airframe interaction noise could explain the discrepancy in the SPL differences.

An order of magnitude argument can be made for the SPL derived at a distance of 16R. If we integrate the pressure distribution over the face of the rotor blade, we get a rough estimate of the thrust. Then if we take, for example, the thrust value of 6.58 N for the isolated rotor at 7000 RPM and assume the other terms cosine and Mach number terms are negligible, we can approximate an acoustic loading pressure of 0.14 Pa. If we assume a sinusoidal signal, which is reasonable considering the waveform of the acoustic pressure plots in Fig. 7, the root mean square (RMS) pressure is 0.1 Pa. This RMS acoustic loading pressure is equivalent to an SPL of 73.9 dB, which is very close to the SPL at the first BPF harmonic for observer 5. Therefore, without taking directivity into account, we are able to validate the magnitude of the simulation results.

V. Conclusion

In this study the aerodynamics and aeroacoustics of the DJI Phantom 3 quadrotor were simulated using CREATE^{TM}-AV Helios and an implementation of Farassat Formulation 1A. mStrand was chosen for the near-body flow solver and was shown to predict thrust well for both the isolated rotor and quadrotor configuration. Although the isolated rotor figure of merit was underpredicted, all computed values were accurate within the bounds of experimental uncertainty.

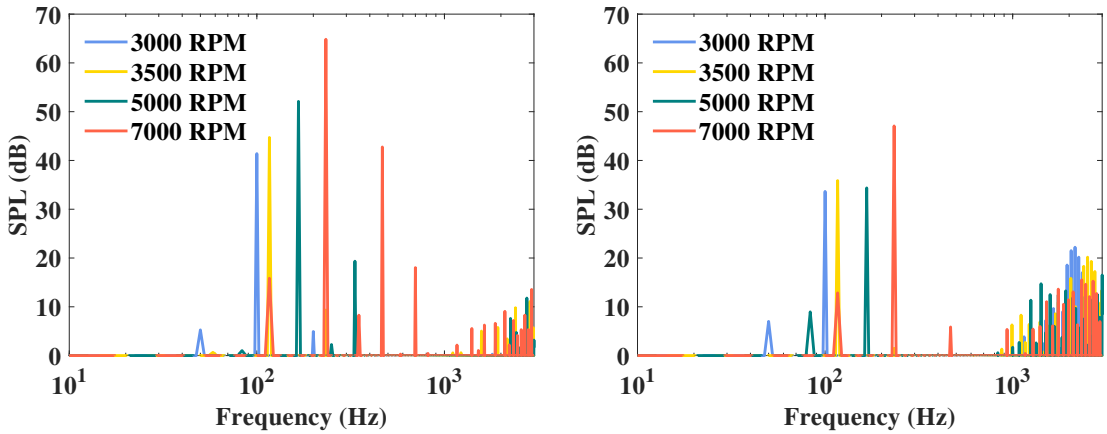

(a) Observer 5 (b) Observer 7

Fig. 9 Sound pressure level in the frequency spectrum.

Therefore this serves as a first validation that the mStrand solver can be used for small quadrotor predictions. The rotor surface pressure distribution was assumed to be steady for the acoustics analysis and a native solver was developed. The acoustic field was shown to agree with previous work in quadrotor sound characterization and the directivity of the thickness and loading components of blade-induced noise.

This study serves as an introduction into acoustic field prediction for quadrotors using the Helios suite. This results of this study were directly comparable to previous work in the literature. However, this work had multiple limitations which could be resolved in future studies. For example, the surface pressure distribution was taken instantaneously from the CFD simulations. Although this is sufficient in obtaining the appropriate order of magnitude in the predictions, the transient effects of the rotor blade, especially at higher Reynolds numbers, will play a role. Two simple possible remedies to this could be computing the average surface pressure values over the rotor revolution or simply using the entire set of pressure distribution. By taking the entire pressure distribution set, the unsteady terms in FF1A will play a role. For the sake of developing a proof of concept for this study, storing only the instantaneous pressure, which requires little computational memory, was deemed appropriate.

In addition, although the flow fields were predicted for both isolated rotor and quadrotor computations, this study only considered the acoustics of isolated rotor. Future studies could expand to quadrotor configurations, as well as trimmed flight noise predictions. There is currently an ongoing research by the U.S. Army Aviation Development Directorate to simulate a quadrotor in RPM-based trimmed flight. The acoustic field of these flight scenarios should be directly related to the surface pressures derived from these simulations. Therefore, it will be interesting to derive the noise generated from a quadrotor in a typical flight situation.

Acknowledgments

Dr. Russell of NASA Ames Research Center shared both the CAD geometry for the rotor and fuselage as well as experimental data from his team's project. Dr. Strawn of the U.S. Army Aviation Development Directorate granted allocation on the Department of Defense High Performance Computing system and facilitated Mr. Thai's participation in the Army's summer internship program. Mr. Jain supervised Mr. Thai's internship and provided the Helios suite training. Professor Brentner shared the PSU-WOPWOP code for use in this research. Henry Jia of U.C. Davis provided guidance on running aeroacoustics simulations. Mark Potsdam provided a lot of insight in understanding and converting the CFD outputs from Helios. Dr. Lakshminarayan, the mStrand developer, provided feedback on running mStrand simulations. Mr. Thai receives funding from the Department of Mechanical Engineering at Boston University.

References

[1] Board, T. R., National Academies of Sciences, E., and Medicine, *Assessing Community Annoyance of Helicopter Noise*, The National Academies Press, Washington, DC, 2017. doi:10.17226/24948.

[2] Skagerstrand, A., Kobler, S., and Stenfelt, S., "Loudness and annoyance of disturbing sounds - perception by normal hearing subjects." *International Journal of Audiology*, Vol. 56, No. 10, 2017, pp. 775–783. doi:10.1080/14992027.2017.1321790.

[3] Intaratep, N., Alexander, W. N., Devenport, W. J., Grace, S. M., and Dropkin, A., "Experimental Study of Quadcopter Acoustics and Performance at Static Thrust Conditions," *AIAA Paper No. 2016-2873*, 2016.

[4] Russell, C., Jung, J., Willink, G., and Glasner, B., "Wind Tunnel and Hover Performance Test Results for Multicopter UAS Vehicles," *AHS 72nd Annual Forum*, 2016.

[5] Russell, C., Willink, G., Theodore, C., Jung, J., and Glasner, B., "Wind Tunnel and Hover Performance Test Results for Multicopter UAS Vehicles," Tech. Rep. TM—2018–219758, NASA, 2018.

[6] Cabell, R., McSwain, R., and Grosveld, F., "Measured Noise from Small Unmanned Aerial Vehicles," NOISE-CON, 2016.

[7] Kloet, N., Watkins, S., and Clothier, R., "Acoustic signature measurement of small multi-rotor unmanned aircraft systems," *International Journal of Micro Air Vehicles*, Vol. 9, No. 1, 2017, pp. 3–14.

[8] Tinney, C. E., and Sirohi, J., "Multirotor Drone Noise at Static Thrust," *AIAA Journal*, Vol. 56, No. 7, 2018, pp. 2816–2926.

[9] Christian, A., Jr., D. D. B., Zawodny, N. S., and Rizzi, S. A., "Auralization of tonal rotor noise components of a quadcopter flyover," *Inter-Noise 2015*, 2015.

[10] Zawodny, N. S., and Jr, D. D. B., "Investigation of Rotor-Airframe Interaction Noise Associated with Small-Scale Rotary-Wing Unmanned Aircraft Systems," *AHS 73rd Annual Forum*, 2017.

[11] Yoon, S., Diaz, P. V., Jr., D. D. B., Chan, W. M., and Theodore, C. R., "Computational Aerodynamic Modeling of Small Quadcopter Vehicles," *AHS 73rd Annual Forum*, 2017.

[12] Diaz, P. V., and Yoon, S., "High-Fidelity Computational Aerodynamics of Multi-Rotor Unmanned Aerial Vehicles," *2018 AIAA Aerospace Sciences Meeting*, 2018.

[13] Zawodny, N. S., Christian, A., and Cabell, R., "A Summary of NASA Research Exploring the Acoustics of Small Unmanned Aerial Systems," *AHS Specialists' Conference on Aeromechanics Design for Transformative Vertical Flight*, 2018.

[14] Theodore, C. R., "A Summary of the NASA Design Environment for Novel Vertical Lift Vehicles (DELIVER) Project," *AHS International Technical Conference on Aeromechanics Design for Transformative Vertical Flight,*, 2018.

[15] Roget, B., Sitaraman, J., Lakshminarayan, V., and Wissink, A., "Prismatic Mesh Generation Using Minimum Distance Fields," *Tenth International Conference on Computational Fluid Dynamics (ICCFD10-219)*, 2018.

[16] Sankaran, V., Wissink, A., Datta, A., Sitaraman, J., Jayaraman, B., Potsdam, M., Katz, A., Kamkar, S., Roget, B., Mavriplis, D., Saberi, H., Chen, W.-B., Johnson6, W., and Strawn, R., "Overview of the Helios Version 2.0 Computational Platform for Rotorcraft Simulations," *49th AIAA Aerospace Sciences Meeting*, 2011.

[17] Wissink, A., Jayaraman, B., Datta, A., Sitaraman, J., Potsdam, M., Kamkar, S., Mavriplis, D., Yang, Z., Jain, R., Lim, J., and Strawn, R., "Capability Enhancements in Version 3 of the Helios High-Fidelity Rotorcraft Simulation Code," *50th AIAA Aerospace Sciences Meeting*, 2012.

[18] Williams, J. E. F., and Hawkings, D. L., "Sound Generation by Turbulence and Surface in Arbitrary Motion," *Philosophical Transactions of the Royal Society, London*, Vol. 264, No. 1151, 1969, pp. 321–342.

[19] Farassat, F., and Succi, G. P., "A review of propeller discrete frequency noise prediction technology with emphasis on two current methods for time domain calculations," *Journal of Sound and Vibration*, Vol. 71, No. 3, 1980, pp. 399–419.

[20] Brentner, K. S., Bres, G. A., Perez, G., and Jones, H. E., "Maneuvering Rotorcraft Noise Prediction: A New Code for a New Problem," *AHS Aerodynamics, Acoustics, and Test Evaluation Specialist Meeting*, 2002.

[21] Farassat, F., "Derivation of Formulations 1 and 1A of Farassat," Tech. Rep. TM–2007–214853, NASA, 2007.

[22] Brentner, K. S., and Farassat, F., "Modeling aerodynamically generated sound of helicopter rotors," *Progress in Aerospace Sciences*, Vol. 39, 2003, pp. 83–120.

[23] Bres, G., Brentnera, K., Pereza, G., and Jones, H., "Maneuvering rotorcraft noise prediction," *Journal of Sound and Vibration*, Vol. 275, 2004, pp. 719–738.

[24] Lee, S., Morris, P. J., , and Brentner, K. S., "Improved Algorithm for Nonlinear Sound Propagation with Aircraft and Helicopter Noise Applications," *AIAA Journal*, Vol. 48, No. 11, 2010, pp. 2586–2595.

[25] Jia, Z., Lee, S., Sharma, K., and Brentner, K. S., "Aeroacoustic Analysis of a Lift-Offset Coaxial Rotor Using High-Fidelity CFD-CSD Loose Coupling Simulation," *AHS 73rd Annual Forum*, 2017.

[26] Walmart, "DJI Phantom 3," , 2019.

[27] Thai, A. D., Jain, R., and Grace, S. M., "CFD Validation of Small Quadrotor Performance using CREATE-AV Helios," *AHS 75th Annual Forum*, 2019.

[28] Thai, A. D., and Grace, S. M., "A Numerical Study of Important Flow Effects for Quadrotor Performance in Hover," *AIAA Region I Student Conference*, 2019.